

Carbon Origami: A Method to Fabricate Lightweight Carbon Cellular Materials

Monsur Islam, Joshua Flach and Rodrigo Martinez-Duarte*

Multiscale Manufacturing Laboratory, Department of Mechanical Engineering, Clemson University, Clemson, SC 29631, USA

Abstract

We present the fabrication of lightweight cellular carbon materials using an origami-inspired technique. Complex, porous shapes are fabricated by carbonizing an origami structure made by pre-creasing and manual folding a flat piece of pure cellulosic paper. This relatively simple process yields carbon origami shapes that feature density as low as $0.014 \pm 0.005 \text{ g/cm}^3$, 0.93% the density of bulk glassy carbon. Yet, the specific stiffness of this carbon origami and its capability to transfer load compare advantageously to other lightweight cellular materials such as carbon nanotube foams, graphene elastomers, metallic microlattices, silica aerogel, and carbon foams. Such promising mechanical properties coupled to the high temperature resistance and excellent chemical and electrochemical stability of carbon positions carbon origami as a candidate to fabricate lightweight, multifunctional materials.

1. Introduction

A cellular material was defined by Gibson and Ashby as an interconnected network of solid struts or plates forming the edges and faces of cells [1]. One can find both nature- and man-made cellular materials with either periodic or stochastic internal structure. Examples of periodic cellular materials found in nature are wood [2] and cork [3]. Trabecular bone [4], plant parenchyma [5] and sponge [6] are few examples of a natural stochastic foam-like structure. In contrast, synthetic materials with stochastic foam-like structure include silica aerogel [7,8], carbon nanotube (CNT)

* Corresponding author

Email address: rodrigm@clemson.edu (R. Martinez-Duarte)

foams [9], graphene elastomers [10], metallic foams, polymer foams [11], and carbon foams [12,13]. Man-made micro- and nanolattices have been reported recently out of different materials [14–17], which represent an excellent example of periodic structures. The most important feature of cellular materials is their much lower density compared to the bulk version of the same material. Additionally, cellular materials offer an improved specific surface area and specific mechanical strength. It is thus no surprise that cellular materials find application as lightweight structural components [18], energy absorption materials [19], catalysts support [20], and performance filters [21]. Cellular carbon materials are reported using different carbon allotropes such as CNT, graphene, glassy carbon and carbons derived from organic precursors [9,10,17,22]. In general, these materials feature interesting properties including low density, high specific compressive strength, high temperature tolerances (~3000 °C in inert atmosphere), high surface area and adjustable electrical and thermal conductivity [23]. Such properties have enabled the use of these cellular carbon materials in thermal energy storage, adsorption of water vapor, electrochemical measurements, heat sinks and catalyst support [22,24]. Here, we are interested on cellular carbon materials derived by heat treating organic polymers. This is mainly due to the facility of shaping the precursor instead of the carbon.

We report on the use of origami techniques to fabricate lightweight cellular carbon materials. In origami, 3D complex architectures are fabricated from a flat piece of paper by folding the paper along prescribed creases [25–27]. Origami is gaining significant scientific and technological interest among the scientific community due to its potential to fabricate numerous intricate architectural shapes of engineering value [28]. Here we emphasize the use of origami structures as lightweight rigid structures. We use cellulose paper with a random structure as carbon precursor. Starting with a flat piece of paper, we use origami techniques to crease and fold specific structures that we then pyrolyze in an inert atmosphere. The resulting carbon origami features a stochastic cellular microstructure and a designed macrostructure with characteristically thin cross section. The carbon origami structures reported here feature a relative stiffness comparable to CNT foams [9], graphene elastomers [10], metallic microlattices [15], carbon foams [13] and silica aerogel [7].

In this work, we present the characterization of the carbon microstructure resulting from carbonizing paper and a discussion of its effect on the mechanical properties of the origami structure. Although we present results using a specific kind of cellulosic paper, there is an immense

potential to tailor the mechanical properties of carbon origami by tailoring the microstructure of the precursor paper. We also address the effect of carbonization on the cellulose fibers and on the origami structure in terms of structural shrinkage. We finish by showcasing the versatility of this technique to make different origami structures of different sizes. The use of origami-based techniques to manufacture carbon cellular materials has excellent scalability prospects. Due to the maturity of the paper making industry, it is possible to produce relatively inexpensive, pure cellulose paper rolls. These could be creased and folded after optimizing continuous embossing and folding techniques, such as those used in the manufacturing of paper bags and paper filters. Continuous heat treatment of the folded shapes can be implemented using belt conveyor or pusher tunnel furnaces, common in the production of tile and other ceramic pieces.

2. Experimental

2.1 Fabrication of carbon origami

The fabrication process consisted of four steps illustrated in Figure 1: 1) design of crease pattern, 2) automatic pre-creasing, 3) manual folding and 4) carbonization. Pure cellulose chromatography papers Fisherbrand Chromatography Paper, Cat. No. 05-714-1 with thickness of 0.19 mm or Whatman 3MM Chromatography paper, Cat. No. 3030-6158 with a thickness of 0.34 mm were used for this work. Although we are able to fabricate different origami patterns, we focused our study on Miura-ori, a pattern that belongs to the family of rigid origami. In this case, the facets are considered as rigid panels and creases are considered as hinges [29,30]. The geometry of Miura-ori resembles a herringbone pattern and consists a series of convex “mountains” and concave “valleys”. This origami tessellation has gained much attention among the engineering communities because of its simplicity and mechanical properties such as high specific stiffness [31,32], impact energy absorption [33,34], and negative Poisson’s ratio [35,36]. The Miura-ori pattern has been employed in different applications including packaging of solar panels for space mission [37] and deformable energy storage devices [38]. The pattern can be also found in nature in different forms such as leaves [39,40], embryonic intestines [41] and insect wings [42].

2.1.1 Design of crease patterns

Fig. 1a shows the crease pattern for a unit cell of a Miura-ori fold. The dotted and solid lines in the unit cell represent the creases to create “valleys” on one side of the paper and “mountains” on the other. The Miura-ori design used here featured 16 unit cells. A unit cell can be defined by the design parameters h , l and α [30]. All the Miura-ori samples fabricated here featured an α of 75° and a 3:5 ratio between h and l . Such specific ratio resulted from fitting 16 unit cells in a square. We only varied the value of h from 3.1 mm (1/8 in) to 15.3 mm (5/8 in) as the size of the pieces increased from 1 inch \times 1 inch to 5 inch \times 5 inch.

Although the focus of this paper was the Miura-ori structure, other origami structures were studied to assess scalability and complexity of the process. We characterized the Waterbomb base and Yoshimura origami structures. These designs also featured 16 unit cells. The Waterbomb base unit cell was defined by the design parameter s . The Yoshimura unit cell was defined by the design parameters x and y (Fig. 7b and 7c).

Individual crease patterns for “valleys” and “mountains” for all origami structures were designed using Solidworks (Dassault Systems, Waltham, MA, USA). Examples of valleys and mountains for Miura-ori are shown in Fig. 1b and c respectively. These design files enabled the automatic pre-creasing detailed in the next section.

2.1.2 Automatic pre-creasing

We used a modified desktop cutting-plotter machine (Graphtec CE6000-40, Japan) to automatically pre-crease the paper and facilitate folding. We replaced the cutting blade with an empty, generic ballpoint pen with a ball diameter of 1.5 mm. Parameters of interest during pre-creasing included speed of movement, acceleration, number of passes and pressing force of the pen. After optimization (data not shown), we defined a speed of 12 cm/s, acceleration of 0.71 m/s^2 , a force of 2.16 N, and three passes as the ideal parameters to achieve the targeted creasing that will facilitate folding of the origami tessellation. An example of the pre-creased paper for Miura-ori in such process is shown in Fig. 1d. Alignment of valleys and mountains was implemented using marks that were automatically generated by the software of the cutting plotter and printed on the paper. Pre-creased samples with any visible misalignment were discarded.

2.1.3 Manual folding

Following Miura-ori techniques, folding was done manually to ensure facets adjacent to the creases for the “valleys” were rotated into the paper, while the facets adjacent to the creases for the “mountains” were rotated out of it [43]. An example of the folded paper Miura-ori is illustrated in Fig. 1e. As indicated in Fig. 1e, the angle obtained after folding, α' , was smaller than designed. Hence, instead of 75° we obtained $43.75^\circ \pm 0.33^\circ$. Five paper Miura-ori were folded for each value of design parameter h .

2.1.4 Carbonization

Once folded, the paper Miura-ori origami structures were carbonized in a tube furnace (TF1400, Across International, USA) using a well characterized protocol [44–47]. Due to a limitation on the size of the tube, the maximum dimension of the samples was 115 mm. The carbonization protocol featured 5 steps: (1) heating from room temperature to 300°C at $5^\circ\text{C}/\text{min}$; (2) dwell at 300°C for 30 min to allow the excess oxygen to escape the furnace; (3) heating from 300°C to 900°C at $5^\circ\text{C}/\text{min}$; (4) dwell at 900°C for 75 min; and (5) cooling down to room temperature at a cooling rate of $5^\circ\text{C}/\text{min}$. Process was done under a nitrogen atmosphere. An example of the resultant carbon Miura-ori is shown in Fig. 1f. Shrinkage occurs, which yields a sharper folding angle, α'' , when compared to the angle α' present after folding.

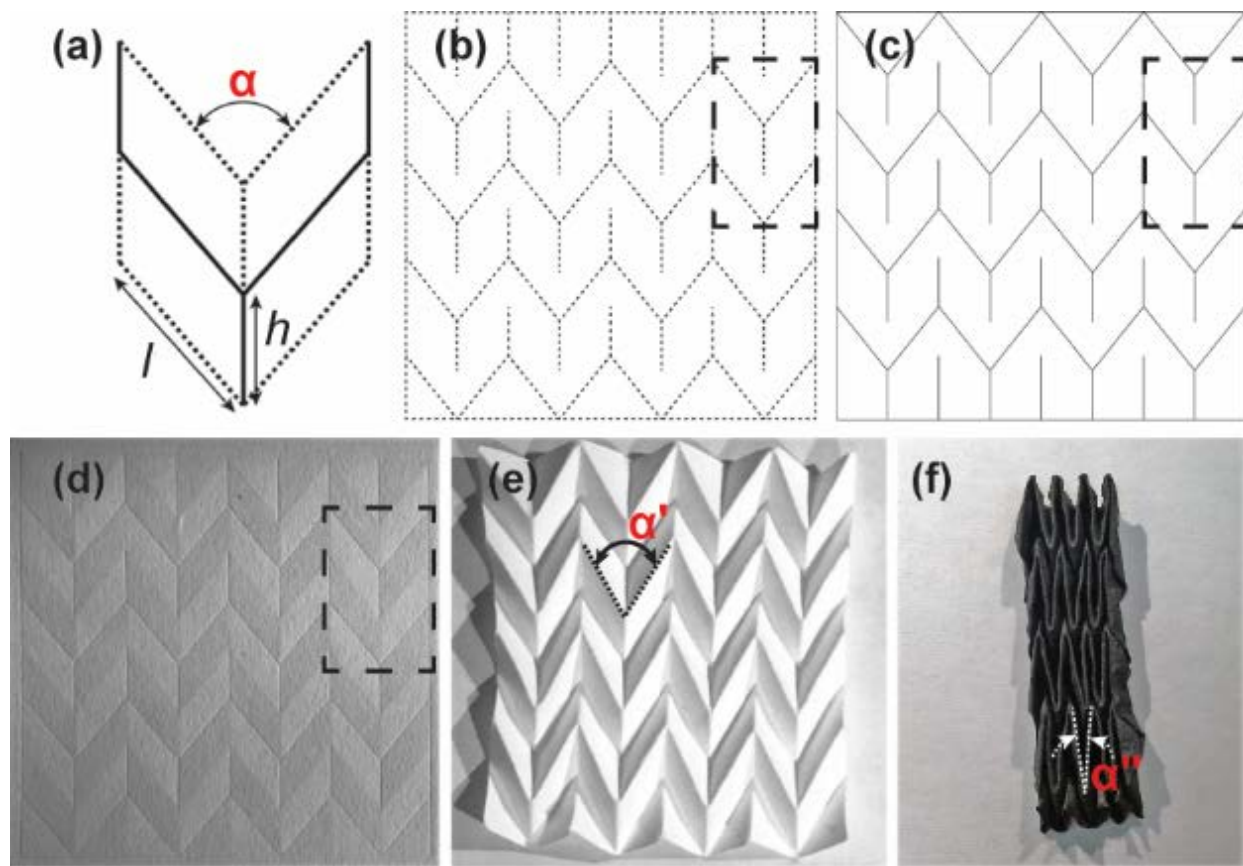


Figure 1: Fabrication process of carbon Miura-ori. (a) Unit cell of a Miura-ori pattern. The dotted lines represent the “valleys” and the solid lines indicate the “mountains”. The unit cell is defined by the characteristic design parameters h , l and α . CAD software was used to create the crease patterns for (b) “valleys” on one side and (c) “mountains” on the opposite side of the paper for fabrication of Miura-ori. (d) Example of a 3 inch \times 3 inch paper creased using a modified cutting plotter. The unit cell of the Miura-ori pattern is indicated by the dashed rectangle, compare to (a). (e) Paper Miura-ori obtained by manually folding the creased paper shown in (d). because of manual folding, the design angle α decreased to the folding angle α' . (f) Carbon Miura-ori obtained by heat treatment of the paper Miura-ori at 900 °C in nitrogen atmosphere. Although shrinkage occurs, the shape is conserved. Because of the shrinkage, folding angle α' decreased to α'' for the carbon Miura-ori.

2.2 Characterization

2.2.1 Material characterization

The carbon miura-ori structure was characterized using X-ray diffraction (XRD, Rigaku Ultima IV, Japan) spectroscopy to determine its crystallographic structure. Thermogravimetric analysis (TGA) was performed to characterize weight loss during carbonization in nitrogen atmosphere with a heating rate of 5 °C/min. The microstructures of both the precursor paper and the resultant carbon were using scanning electron microscopy (SEM, S4800, Hitachi, Japan). A thin carbon film (10 nm) was sputtered on the precursor paper to facilitate its imaging. The microstructure of the carbonized paper was further analyzed by high resolution transmission electron microscopy (HRTEM, H9500, Hitachi, Japan). The pore size distribution of the carbonized paper was characterized by image analysis of the SEM images using the particle analyzer, an inbuilt macro in the ImageJ software.

2.2.2 Structure characterization

Following current practices in cellular materials, the structural density (ρ) of the carbon Miura-ori structures was determined by the envelop method, which is the ratio between the mass of the carbon Miura-ori and the total volume it occupied [9,48]. The compression tests of the carbon Miura-ori structures were performed at a rate of 1 mm/min to 80% strain using an Instron Single Column Testing System (Model 5944). A load cell of 50 N was used for the compression tests. The stress-strain curve obtained in the compression test had three distinct regions: the elastic region, post-yielding softening and densification [49,50]. We calculated the compressive strength (σ_m) of the carbon Miura-ori sample as the onset point of fracturing of the panels, and the elastic modulus (E) as the slope of the elastic region of the stress-strain curve. This elastic region is characterized by the fact that the panels can stretch away from the creases to absorb the compression force.

3. Results and Discussion

3.1 Compressive strength and Elastic Modulus depending on structural density

The structural density (ρ) of different carbon Miura-ori structures is plotted in Fig. 2a for different lengths of the characteristic dimension h of a Miura-ori unit cell (see Fig. 1a). The density

decreases from 0.03 ± 0.004 to 0.014 ± 0.005 g/cm³ as h increases from 6.12 to 12.24 mm. An h of 6.12 mm is currently the smallest dimension we can fabricate with our current setup (see section 3.4). The density of the structure as measured with the envelope method shows strong dependence on the length of h and hence size of the panel. This suggests that deformation of the structure during shrinkage and possibly elimination of byproducts during carbonization play an important role on determining the density of the carbon Miura-ori. These mechanisms are discussed in the shrinkage section (Section 3.3). In this current section, we present the density values to emphasize the potential of carbon Miura-ori as a lightweight material. The structural density of the carbon Miura-ori obtained here ranges from 0.93% to 2% of the density of bulk glass-like carbon (1.3-1.5 g/cm³ [51]).

The results from the characterization of σ_m and E are shown in Fig. 2b. As expected, σ_m and E increase with the increase in density of the carbon Miura-ori. The value for σ_m increased from 4.12 ± 1.29 kPa for $\rho = 0.014$ g/cm³ to 15.85 ± 2.21 kPa for $\rho = 0.03$ g/cm³. The value of E increased from 49.37 ± 6.24 kPa for $\rho = 0.014$ g/cm³ to 193.83 ± 32.17 kPa for $\rho = 0.03$ g/cm³. Hence, σ_m and E are also inversely proportional to the design parameter h . In comparison, the average compressive strength of bulk glass-like carbon is in the range 300 – 700 MPa [52,53].

Cellular materials, including stochastic foams, can be characterized by the dependence on density of elastic modulus given by Gibson and Ashby's scaling law (Equation 1) [54]:

$$E \propto E_S(\rho/\rho_S)^n \quad (1)$$

where E_S and ρ_S are the elastic modulus and the density of the solid respectively, and n is an exponent that represents the mode of deformation, e.g. bending or stretching [55]. The value of the constant n depends on the microstructure of the material as well as the structural geometry which includes the cell type (open or closed), the geometrical arrangement of the cells and the size of the cells [56]. Values of n beyond 2 represent rapid loss of interesting properties as density increases and signifies inefficient load transfer between the ligaments of the cellular structure [15]. Values of n less than 2 signifies better load transfer capability through the structure ligaments. A $n = 1$ denotes a stretch dominated structure, which exhibits higher compressive strength and stiffness in comparison to bending-dominant structures ($n = 2$) [55]. Plotting the relative elastic modulus, E/E_S , versus their relative density, ρ/ρ_S , shows that the Carbon Miura-ori origami

structures features a $n = 1.76$ when considering the values for E_s and ρ_s as 20 GPa and 1.5 g/cm^3 for glass-like carbon respectively [17,57] (Fig. 2c). This value is close to 2 which suggests a bending-dominant mechanical behavior similar to open cell cellular materials [1]. This was expected for Miura-ori because of the random collection of $5.26 \pm 2.53 \text{ }\mu\text{m}$ -thick fibers in the facets. Furthermore, Miura-ori in particular does not feature any strut at its basal plane, as in the case of octet-trusses for example [14], which is a characteristic for stretch-dominated microlattices [58]. A $n = 1.76$ also means that the carbon Miura-ori exhibits better scaling and better load transferring capability than other cellular materials with higher values of n . For example, silica aerogel and carbon nanotube (CNT) foams used for catalysts supports and energy storage applications respectively feature a $n = 3$ [7,9]. Carbon aerogels derived through carbonization of resorcinol-formaldehyde aerogel at $1100 \text{ }^\circ\text{C}$ feature a $n = 2.7$ at a porosity ranging from 80% to 95% [13]. Metallic microlattices feature a $n = 2.4$ [15], while graphene foams display a $n = 2.5$ [10]. Hence, the carbon Miura-ori structures presented here compare advantageously to other common lightweight cellular materials in terms of scaling and load transfer capabilities. However, the compressive strength of the carbon Miura-ori structures (4.12 kPa – 15.85 kPa) feature less compressive strength than other structural materials with similar density such as metallic microlattices (70 kPa – 3 MPa) [14] and carbon foam ($\sim 50 \text{ kPa}$) [13]. We hypothesize that the random distribution of the open pores among the carbon fibers and the high standard deviation of the fiber diameter are the reason for the low compressive strength. We provide further details on the microstructure of the carbon fibers in section 3.2. Ongoing work is on using different pure cellulose films with different microstructures. The control over smaller scales is expected to yield a significant increase in compressive strength as recently reported by other authors [59].

Paper manufacturing involves pulping of wood chips followed by chemical treatment of the pulps, mechanical pressing, and drying [60]. The microstructure of paper, i.e. fiber dimension and spatial arrangement, depends on the source of the wood pulp, pulping method, treatment of the pulp and the mechanical pressing [61]. Different microstructure of the paper can be obtained by controlling these processing steps. For example, fibers from softwood feature slenderness ratio (length/diameter) ranging from 95 to 120, whereas fibers from hardwood have slenderness ratio ranging from 55 to 75 [61]. Higher slenderness ratio translates to a higher density of paper and lower pore size distribution. Furthermore, paper made from thermomechanical pulping possesses 25-40% higher porosity than that made from chemical pulping [62]. The maturity of the paper

industry represents an excellent stepping stone towards manufacturing carbon origami of tailored properties. Once paper is obtained with specific microstructural properties, the continuous processing for carbon origami will be enabled.

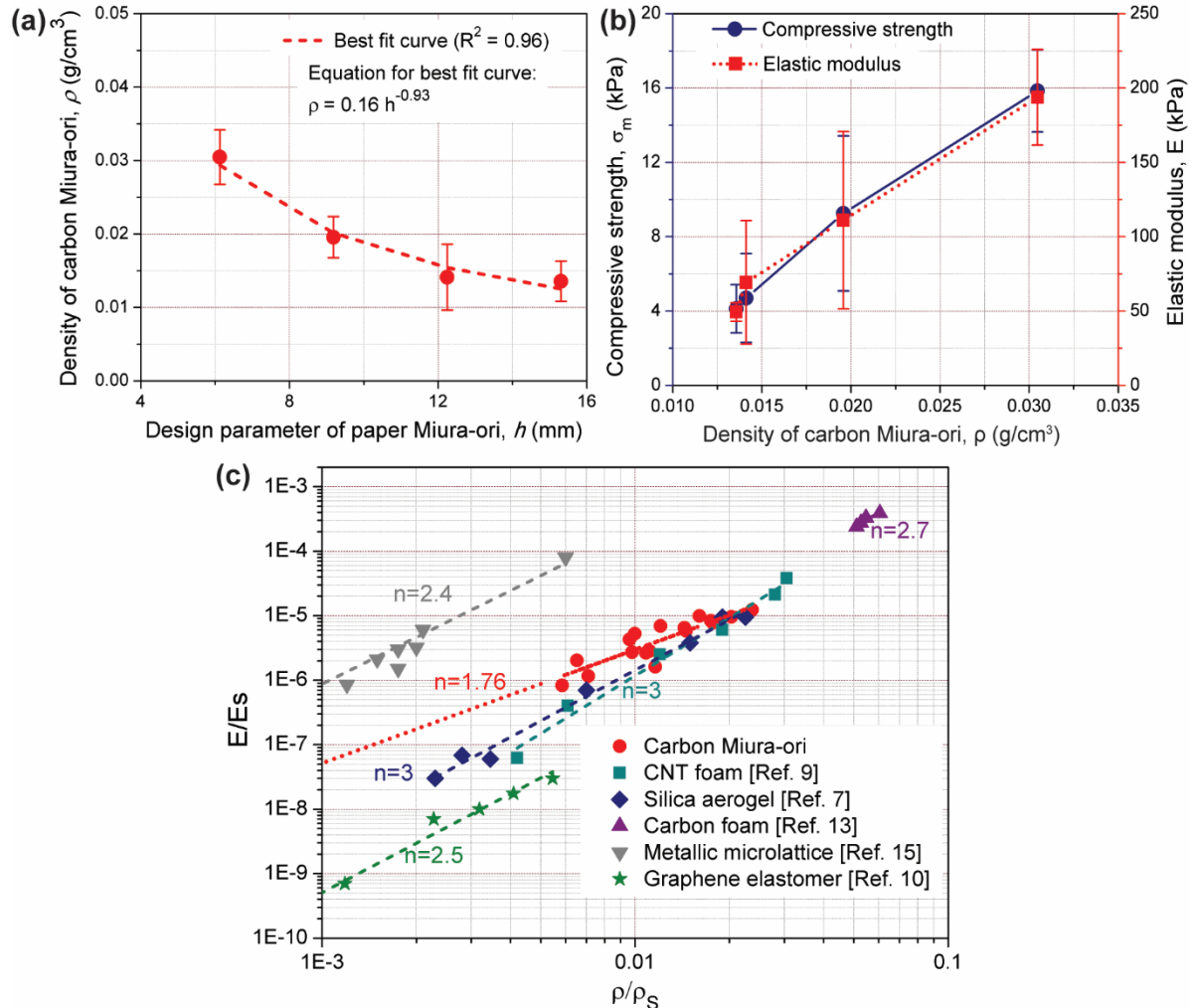


Figure 2: (a) Density (ρ) of carbonized Miura-ori of different sizes. At least five Miura-ori were characterized for the shrinkage and the density for each value of h . The error bars represent the standard deviation in the measurement. The red dashed line represents the best fitted curve to the density. (b) Plots of compressive strength (σ_m) and elastic modulus (E) against density of the carbonized Miura-ori. The large standard deviations are attributed to the random distribution of carbon fibers. (c) Relative elastic modulus (E/E_S) of carbonized Miura-ori with comparison to other low-density materials.

3.2 Characterizing the microstructure of carbon origami

The results from the XRD characterization of the carbonized paper (Fig. 3) show weak and broad peaks centered around $2\theta = 24^\circ$ and $2\theta = 43^\circ$, which are the characteristics of (002) and (100) reflections of amorphous carbon [63,64].

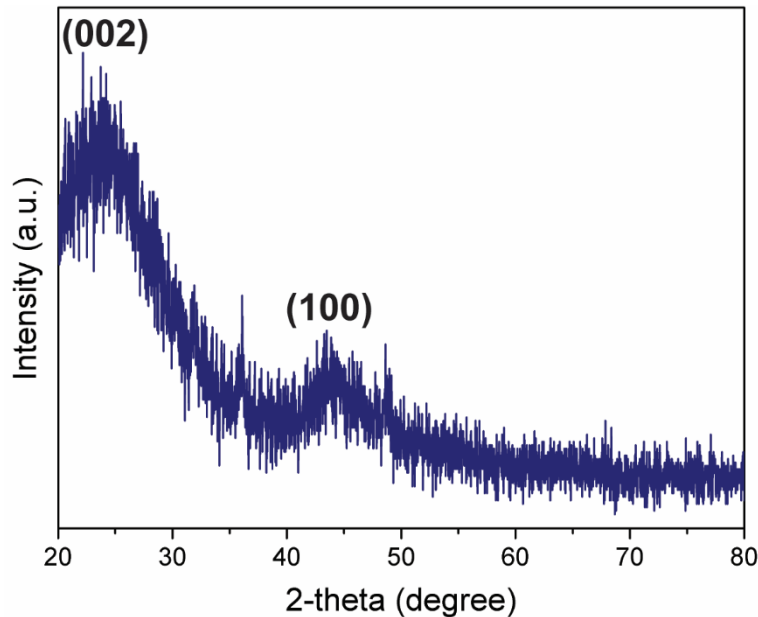


Figure 3: XRD of the carbonized chromatography paper. The presence of peaks at 24 and 43° indicate amorphous carbon.

The chromatography paper used in this work was basically a collection of tightly packed cellulose fibers as shown in Fig. 4b. The average diameter of these fibers was $17.48 \pm 3.06 \mu\text{m}$. The carbon obtained after heat treatment is shown in Fig. 4b. No impurities were observed on the carbon matrix. This in contrast to significant impurities reported when carbonizing other paper types which are not marketed as pure cellulose [65]. The fibers shrank to an average diameter of $5.26 \pm 2.53 \mu\text{m}$, resulting on an average linear shrinkage of fiber diameter of $69.89 \pm 5.59\%$. The spacing between fibers is of random nature leading to macroporosity of varying dimensions in the range from $1.56 \mu\text{m}$ to $21.71 \mu\text{m}$ (inset of Fig 4b). The mechanical properties of a material are known to depend on its microstructure [66]. Hence, the compressive strength (σ_m) and elastic modulus (E) of the carbon Miura-ori would depend on the fiber composition, diameter and spacing between them. We hypothesize that the high standard deviation in the carbon fiber diameter and random

and wide distribution of the open pores caused the high standard deviation in σ_m and E as seen in Fig 2b. An improvement of mechanical properties is to be expected if using a fiber matrix with smaller fiber diameter, as reported by other authors [66–68]. Use of smaller fibers can enhance packing in the matrix, thus yielding smaller pores between fibers. Ongoing work is on elucidating the impact of using different cellulose matrices as carbon precursors.

The carbon fibers themselves display a wide range of open pore sizes. SEM analysis at magnification of 120k revealed a mesoporous structure with pore diameter ranging from 3.15 nm to 44.78 nm (Figure 4c). TEM studies at magnification up to 500k further suggested presence of micropores (pore diameter < 2 nm) within the fibers (Figure 4d). However, at the presented scale, it is hard to identify and measure the size of the micropores. Further studies using nitrogen adsorption-desorption will be needed to properly characterize these micropores. Our hypothesis is that the escape of gaseous substances during carbonization causes these micropores in the carbon material and the compact aggregation of these material results in the mesoporous structure. This hypothesis is in accordance with previous reports on synthesis of porous carbon from biopolymer precursors [45,69,70]. These micro- and mesopores also contribute to the microstructure and mechanical properties of the carbon Miura-ori. With increased micro- and mesopores, the carbon fibers become less dense resulting in a decrease in σ_m and E [71]. We expect the micro- and mesoporosity to be increased by augmenting the carbonization temperature. The use of carbonization temperatures up to 1000 °C has been shown to enhance material release during carbonization and yield a material with increased micro- and meso-porosity [72].

The electron diffraction analysis performed during TEM revealed no spots or rings that correspond to any crystal plane (inset of Figure 4d). This supports the previous finding from XRD about the amorphous nature of the carbon sample.

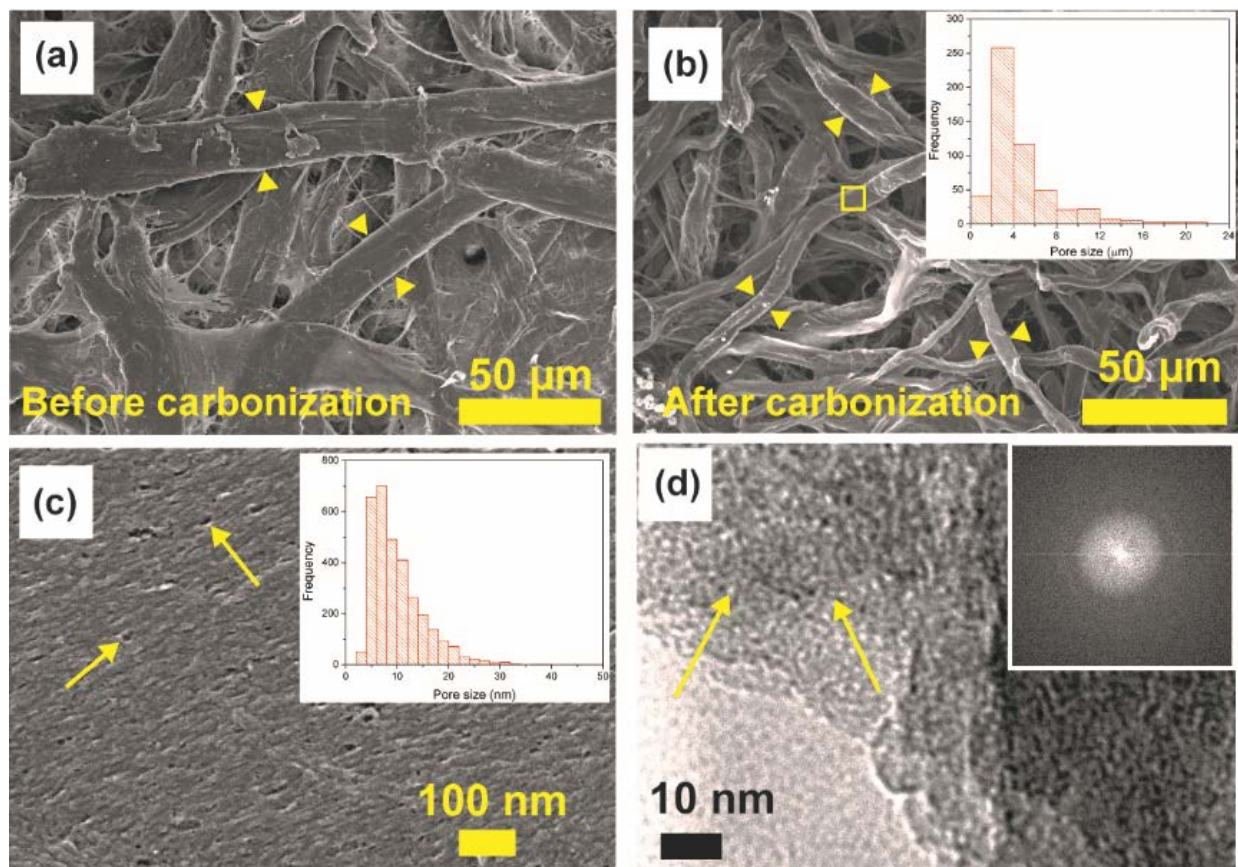


Figure 4: FESEM image of chromatography paper (a) before and (b) after carbonization at a magnification of 600X. The arrows indicate the diameter of the fibers. Diameters were measured for at least ten fibers in both cases. The average diameter of the cellulose fibers in (a) was $17.48 \pm 3.06 \mu\text{m}$ and that for carbon fibers in (b) was $5.26 \pm 2.53 \mu\text{m}$, resulting in an average linear shrinkage of fiber diameter of $69.89 \pm 5.59 \%$. Inset of (b) represents the pore size distribution of the open pores. The diameter of the open pores ranges from $1.56 \mu\text{m}$ to $21.71 \mu\text{m}$. (c) High magnification FESEM image of the carbonized chromatography paper at a magnification of 120k showing the mesoporous structure of the carbon fibers. Representative examples of the pores are indicated by the arrows. Pore diameter ranges from 3.15 nm to 44.78 nm as shown in the inset. (d) HRTEM image of the carbonized chromatography paper showing the micropores in the carbon material. Examples of the micropores are indicated by the arrows. The electron diffraction pattern in the inset shows no ring or spot, which confirms the amorphous nature of the carbon sample.

3.3 Structural shrinkage

Thermogravimetric analysis (TGA) was performed to calculate the carbon yield of chromatography paper. The results from the TGA are shown in Fig. 5 and are in accordance with other authors [73–76]. A sharp weight loss occurs between 300 °C and 380 °C, which is attributed to the thermal decomposition of cellulose in form of volatile components such as levoglucosan, hydroxyacetaldehyde, acetol, CO and CO₂ [77]. Above 380 °C, a gradual weight loss at approximately 0.0097%/°C can be observed which is mainly caused by elimination of oxygen and hydrogen in the form of CO, CO₂ and C_xH_y [78]. The carbon yield at 900 °C in nitrogen atmosphere for the chromatography paper used here is 4.4%, which is in agreement with previous reports [65]. Other types of paper, such as printing paper and Whatman filter paper, were reported to feature a yield in the range of 3 – 23% [65,77]. The yield of 4.4% may seem to conflict with the ~70% linear fiber shrinkage reported above. The theoretical linear shrinkage of the diameter of a solid carbon fiber derived from cellulose is expected to be 79% when considering a 4.4% carbon yield and assuming similar densities for both carbon and cellulose [79,80]. This value can be obtained by equating the mass of a cellulose fiber per unit length (cross-sectional area times density) with that of a carbon fiber featuring a diameter 0.044 times of the cellulose fiber. However, such calculation does not consider the porosity of the fibers illustrated in Fig. 4. We expect the porosity to account for the difference between the theoretical 79% and the observed 70% linear shrinkage. Further studies are required to fully characterize the porosity and exact density of both cellulose and carbon fibers.

The carbon yield is expected to change according to the heating environment. Inert gases commonly used for carbonization include helium, nitrogen, argon and forming gas (Nitrogen and 5% Hydrogen). Su and Lua reported that the thermal conductivity of the gas has an important role on the carbon yield [59]. They determined the convection heat transfer coefficient of helium, nitrogen and argon using an equation correlating Nutshell number with Prandtl number at a volume flow rate of 11.3 ml/min and an inside diameter of 23.55 mm for the tube furnace [59,81]. At 800 °C, they calculated the convection heat transfer coefficient of helium, nitrogen and argon to be 109.20, 18.89 and 12.79 W/m²K respectively. This suggests that a helium environment will result in a lower carbon yield when compared to nitrogen and argon environments. Furthermore, Dickens reported that the use of vacuum facilitates the evacuation of carbonization byproducts when

compared to the use of inert gas atmospheres; which would translate to a lower carbon yield as well [82]. Further work is needed to determine the convection heat transfer co-efficient of different gases for our system and characterize the weight loss in such heating environment for Miura-ori.

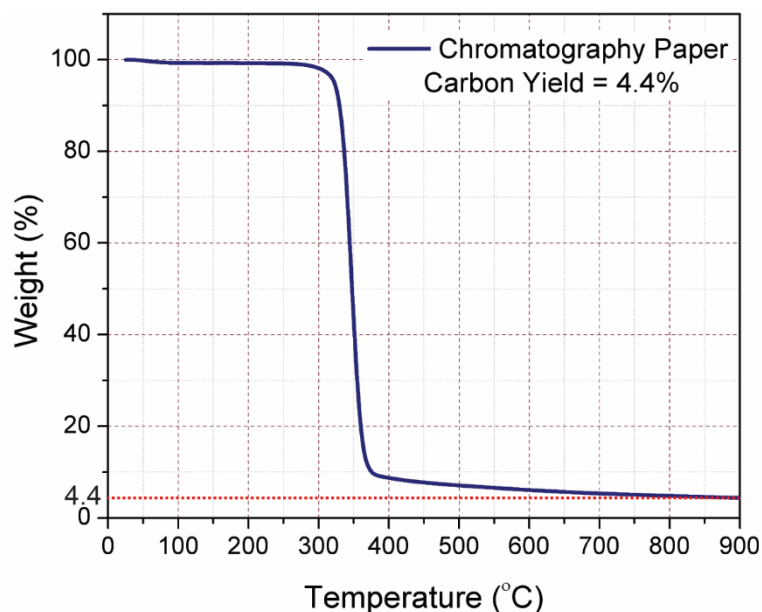


Figure 5: TGA of chromatography paper with a heating rate of 5 °C/min in nitrogen atmosphere. Around 90% weight loss occurs in the range 320 °C – 380 °C. A 4.4% carbon yield was obtained at 900 °C.

The structural shrinkage of the Miura-ori structure is the result of processes at various length scales: from micrometric fibers to centimetric structures. As a reference, the carbonization of a flat piece of paper without the Miura-ori structure resulted in a curved carbon film (see insert in Fig. 6a). The possible reasons for such curved film include induced pressure by the volatile products and associated swelling or blistering during the heat treatment, and the thermal contraction that results during cooling [83–85]. We further speculate that the random distribution of the fibers causes unequal stresses within the fibers during carbonization. However, further investigation is needed to understand such phenomena. Remarkably, a paper piece of the same dimensions but shaped as Miura-ori does not curve during carbonization (Fig. 6a). Our hypothesis is that the dynamics of the Miura-ori structure facilitates the release of thermal stress and thermal contraction

through shrinkage, which prevents it from curving. Interestingly, the amount of shrinkage in different axis of the Miura-ori is different as shown in Fig. 6a. We calculated shrinkage using Equation 2, where L_{Pi} and L_{Ci} are the dimensions of the paper Miura-ori and carbon Miura-ori respectively in the i -axis. Most of the shrinkage occurs on the horizontal plane and in the direction perpendicular to the characteristic dimension h . We denoted this direction as the Y-axis. The least shrinkage happens in the X-axis, or the direction parallel to h . The shrinkage in X with respect to h is constant, slightly variable in the case of Y-axis and significantly different for the Z-axis.

$$\text{Shrinkage (\%)} = \frac{L_{Pi} - L_{Ci}}{L_{Pi}} \quad (2)$$

The material loss during carbonization results in shrinkage of the fibers and this can be explained by the elimination of byproducts from carbonization. We hypothesize that the origami structure has an impact on the evacuation of byproducts. This is because the weight of a carbonized piece of paper with the same dimension than the one used for Miura-ori but without creasing and folding is 10–20% less than the carbon Miura-ori. During carbonization, the decomposition of cellulose produces condense-phase product, which evaporates. The nitrogen gas flowing in the tube aids the evaporation of the byproducts by increasing the mass transfer co-efficient [86]. However, in the case of Miura-ori, it can be possible that the nitrogen gas cannot reach the intricate parts of the Miura-ori uniformly. For example, disturbances in the laminar flow in the tube can be introduced at the folding corners. This results in inefficient mass transfer from those intricate parts and volatile intermediates may get enough time to crosslink and stay as a part of the solid. Therefore, a higher mass is obtained for the carbon Miura-ori. Future work will be required to support this hypothesis and characterize this phenomenon further.

The dynamics of the Miura-ori structure are likely to play a role in shrinkage. It is known that a Miura-ori structure offers the least mechanical resistance in the Y-axis, followed by the Z-axis and lastly the X-axis. The shrinkage reported here follows this trend in all samples (Fig. 6b). Shrinkage of the fiber network during carbonization leads to pulling stresses that find the least resistance in the Y- and Z-axis. Shrinkage also depends on the characteristic dimension h . As h increases, the shrinkage in Y-axis slightly decreases and Z-axis slightly increases. The characterization of the fold angle after carbonization (α'') of Miura-ori structures exposes the fact that α'' is directly proportional to h (Fig. 6b). Hence, the unit cell of a Miura-ori is elongated during carbonization

and this elongation increases as h decreases (plot of α'' in Fig. 6b). According to the geometry of Miura-ori, the dimension in Y-direction is directly proportional to α'' and the dimension in Z-direction is inversely proportional to α'' [36]. Hence, the dimension in Y-direction increases with h resulting in decreasing shrinkage, whereas the dimension in Z-direction decreases with the increase in h resulting in higher shrinkage. The results obtained here suggest a plateau on the folding angle value α'' for $h > 12.2$ mm. However, further experiments in a bigger furnace than ours are required to conclude on this. In order to assess the effect of the thickness of the precursor paper, we compared the dimensions of i) paper Miura-ori folded with chromatography paper of 0.19 or 0.34 mm and the ii) resultant carbon origami after similar heat treatment of both paper Miura-ori. The dimensions in paper were similar, and the amount of shrinkage during carbonization remained the same in all directions regardless of the paper thickness (data not shown). Since both papers featured similar pure cellulose fibers and fiber density, our hypothesis is that the fibers experience similar material loss and thermal contraction force during the heat treatment irrespective of the paper thickness.

The shrinkage behavior detailed above helps explain the decreasing density of the carbon Miura-ori as h increases. An increasing value of h means that the size of the panels of the paper Miura-ori structure increases. This effectively decreases the density of the Miura-ori by introducing larger voids in the structure. Furthermore, shrinkage during carbonization results in retraction of the panels towards each other, caused by the reduction of the folding angle as h decreases. The angle between panels in the vertical plane is $44.08^\circ \pm 7.81^\circ$. The bigger the reduction on the folding angle is, the higher the density of the structure becomes. Hence, small values of h yield increased values of structural density. The plateau in α'' in Fig. 6b results in a plateau in structural density reflected in Fig. 2a. As mentioned before, further experiments are needed with Miura-ori structures with $h > 16$ mm to validate this observation.

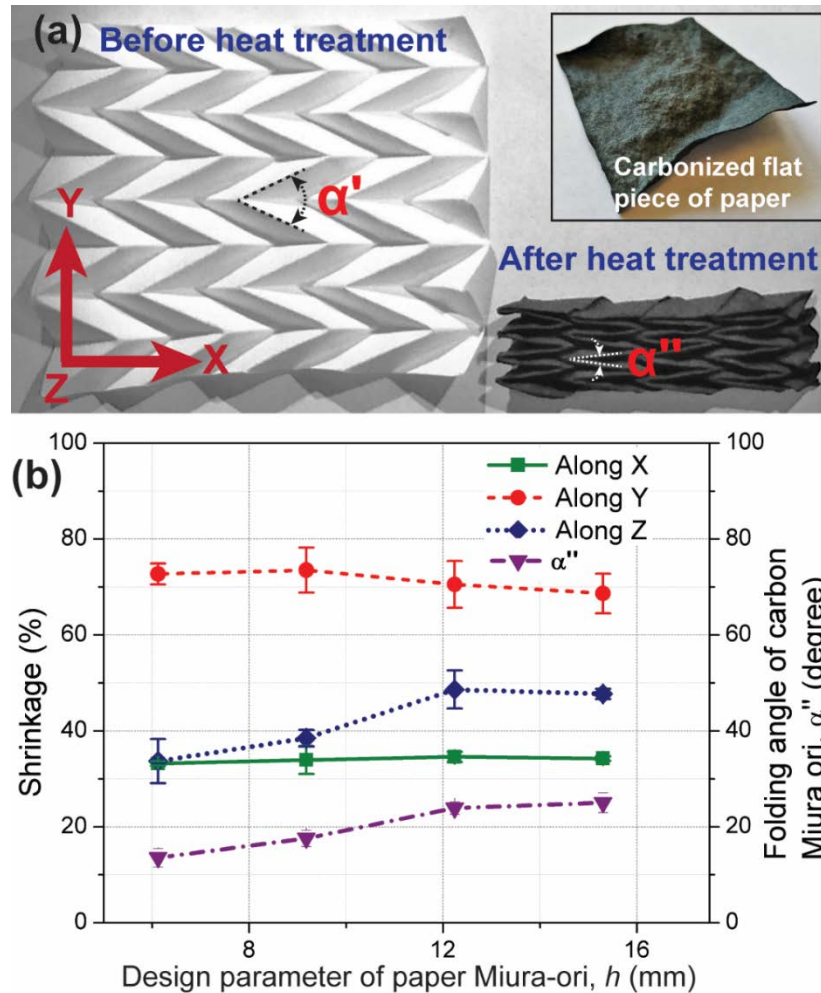


Figure 6: (a) Miura-ori before and after heat treatment. Note that the carbon structure retained the Miura-ori pattern, whereas carbonization of a flat piece of paper results in a randomly curved piece of paper as shown in the inset. Shrinkage occurs during the carbonization. In case of carbon Miura-ori, maximum shrinkage occurs along Y-axis, followed by X- and Z-axis. (b) Shrinkage in X-, Y-, and Z-direction for different sizes of Miura-ori. Maximum shrinkage occurred in Y-direction followed by Z- and X-direction. The folding angle of the carbon Miura-ori (α'') was also plotted for different sizes of Miura-ori. The error bars represent the standard deviation in the measurement.

3.4 Versatility of the fabrication process

We performed studies to elucidate the minimal dimensions achievable in different origami structures when using the manual fabrication technique presented here. The ultimate goal is to automate folding techniques and this initial study is aimed at identifying challenges towards this

goal. Previous authors attributed the failure of folding Miura-ori to the occurrence of folding defects such as curl, crimps and kinks in the facets, which were due to bending and compressive stresses exerted on the facets during manual folding [87]. Here we focused on elucidating the impact of shape complexity on the minimal origami dimensions that are achievable by an average human folder. We studied Miura-ori, Waterbomb base and Yoshimura (Fig. 7) to account for different complexities. The upper limit on dimensions was given by the diameter of the furnace tube used in this work (120 mm). Pre-creasing was achieved across all dimensions tested here since the resolution of the pen, 1.5 mm, was smaller than the separation between all lines.

The complexity of the origami structure can be characterized by N , which is the ratio between the number of crease lines and the area of paper. Miura-ori is the most complex, with highest N , shape among the three studied here followed by Waterbomb base. This means that for a given paper area, a Miura-ori fold features more crease lines. N can then be related to the characteristic size of the different origami structures as given by their unit cell. In this work, the unit cell of Miura-ori is characterized by h , the Waterbomb base by s and Yoshimura by y . For a given length of h , s and y , a Miura-ori features a higher N . Results (Fig. 7d) indicate that the achievable structure depends on the attempted shape and the characteristic size of its unit cell. The minimal length of the characteristic dimension to achieve an origami structure depends on the shape. A value of $h \leq 4.6$ mm was not achievable in Miura-ori, while values of $s \leq 3.6$ mm and $y \leq 2.1$ mm were not possible with Waterbomb based and Yoshimura respectively. In other words, Miura-ori requires the largest size of paper area among the three shapes for a specific N . A value of N greater than 0.05 mm^{-2} failed for all the three shapes during the manual folding. At such value of N , the number of crease lines per unit area of paper becomes so high that the distance between adjacent creases becomes extremely close for manual folding. At such condition, the fold propagates beyond the prescribed crease lines during manual folding and interferes with other adjacent crease lines. This results in folding defects such as curl, crimps and kinks in the facets.

The upper limit of scalability for paper creasing in our case is entirely dependent on the capabilities of the cutting plotter used to pre-crease the paper. The cutting plotter used in this experiment features a maximum cutting area of $375 \text{ mm} \times 50 \text{ m}$. This large cutting area can permit large patterned sheets to be created using the pre-creasing method as long as the features are scaled to the appropriate size. However, large sheet of paper may be more difficult to control, especially

during manual folding of the complex origami structures. In future large-scale manufacturing, the manual folding can be avoided by using upcoming reprogrammable robots [88–90] or processes akin to those used in the manufacturing of paper bags and filters [91]. This will eliminate the dependence of dexterity of the user and likely allow for defect-free folding of the creased paper. It could also allow for fabrication of origami shapes having $N > 0.05 \text{ mm}^{-2}$ and afford better control while handling large sheets of paper. The use of embossing rollers [92–94] to automate the continuous creasing of paper, and the use of rolling furnaces to carbonize origami structures complement automatic folding towards large-scale manufacturing of carbon origami. Rolling furnaces are already common practice in the manufacturing of tiles and other ceramic parts [95].

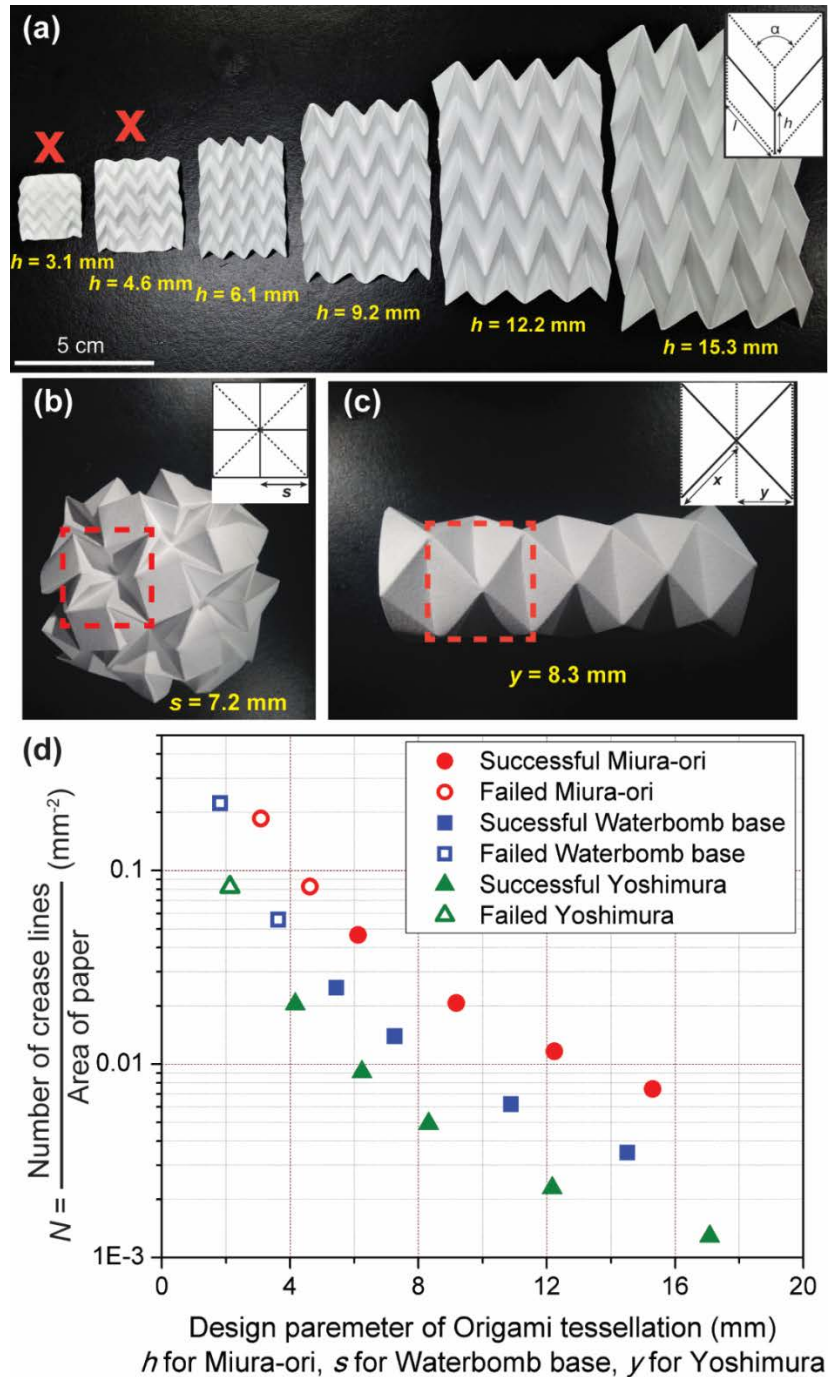


Figure 7. (a) Paper Miura-ori with different value of design parameter h . The Miura-ori with red cross at the top represents the failed attempts. In case of a failed structure, folding defects such as curl, crimps and kinks occurred due to bending and compressive stress exerted on the facets during the manual folding. (b) Waterbomb base and (c) Yoshimura were folded to characterize the effect of complexity on scalability. Unit cells of each origami structures are shown in the inset of

corresponding images and denoted by the red dotted square in the folded paper structures. The number of crease lines per unit area of paper represents the complexity of the origami structures. (d) Ratio of number of crease lines over area of paper were plotted for different sizes of Miura-ori, Waterbomb base and Yoshimura. Note that manual folding fails over a number of crease lines to area of paper ratio of 0.05 mm^{-2} .

4. Concluding remarks

In this work, we demonstrated the fabrication of lightweight, rigid carbon cellular materials using origami techniques. We automated the pre-creasing of flat pieces of cellulosic paper to facilitate the manual folding of origami structures. 3D complex origami shapes of carbon were obtained after carbonization. These featured a unique hierarchical porous microstructure as characterized by SEM and TEM. Shrinkage occurred both in the micro- and macro-scales during the carbonization due to the release of carbonization byproducts. The shrinkage in the macro-scale also depended on the dynamics of the origami shape. The carbon structures featured low density, comparable to other materials such as CNT foams and graphene elastomer that require more complex fabrication processes. The Miura-ori cellular material displays a bending dominant failure under compression ($n = 1.76$). The carbon Miura-ori exhibited low absolute compressive strength and elastic modulus due to the random and wide distribution of the open pores. However, it featured better scaling of relative stiffness when compared to other cellular engineering materials such as silica aerogel, carbon aerogel, graphene elastomers, metallic microlattices and CNT foams. This indicates better load transfer capability of the carbon Miura-ori when compared to these other cellular engineering materials. The large scale manufacturing of carbon origami is envisioned to include embossing rollers to pre-crease the paper, automatic folding using robots and continuous heat treatment using rolling furnaces.

We postulate carbon origami as a technique to fabricate multifunctional cellular materials. Here we demonstrated the initial mechanical properties of carbon Miura-ori structures. Further work is necessary to improve these properties by controlling the microstructure of the carbon by tailoring the structure of the precursor paper and heating protocols. The use of porous carbon in energy applications such as batteries, fuel cells and capacitors is well known. In fact, cellulose derived

carbon by itself or functionalized with metallic nanoparticles has been shown to have excellent electrochemical responses preferable for applications such as batteries, capacitors, CO₂ reducers and fuel cells [96–99]. Further work to elucidate the effect of processing on the surface area and electrochemical properties of carbon origami is necessary. Such studies will also further the use of porous carbon for sensing [98]. The combination of the results emanating from electrochemical and mechanical studies can lead to the development of origami structures with tailored mechanical, energy and sensing properties. For example, lightweight structural capacitors and batteries that are capable to sustain a mechanical load and can monitor their environment. The fact that such carbon material has excellent chemical inertness and can sustain temperatures up to 500 °C under oxidative environments [100] and up to 2500 °C in inert conditions [23] suggests their use in harsh, high temperature applications such as structural filters in diesel engines [101] and during the processing of certain molten materials [102].

Acknowledgements

The authors acknowledge financial support from the Creative Inquiry program in Clemson University project #792. Monsur Islam acknowledges support from Hitachi through a High Technologies Fellowship. The authors are grateful to several colleagues at Clemson University: Dr. Taghi Darroudi from the Electron Microscopy (EM) Laboratory for his advice during image acquisition; Dr. Laxmikant Saraf also from EM lab for his support of this work; Dr. Kimberly Ivy from the Analytical Measurement Laboratory for facilitating TGA studies; Dr. Suyi Li from Mechanical Engineering for discussion about origami designs; and to the Institute for Biological Interfaces of Engineering for facilitating the mechanical testing.

References

- [1] L.J. Gibson, M.F. Ashby, Cellular solids: Structure and properties, Second Edi, Cambridge University Press, Cambridge, 1997.
- [2] K. Ando, H. Onda, Mechanism for deformation of wood as a honeycomb structure I: Effect of anatomy on the initial deformation process during radial compression*, J Wood Sci. 45 (1999) 120–126. doi:10.1007/BF01192328.

- [3] L.J. Gibson, K.E. Easterling, M.F. Ashby, The structure and mechanics of cork, *Proc. R. Society London A*. 377 (1981) 99–117.
- [4] D. Chappard, M.F. Baslé, E. Legrand, M. Audran, Trabecular bone microarchitecture: A review, *Morphologie*. 92 (2008) 162–170. doi:10.1016/j.morpho.2008.10.003.
- [5] J.D. Gray, P. Kolesik, P.B. Høj, B.G. Coombe, Confocal measurement of the three-dimensional size and shape of plant parenchyma cells in a developing fruit tissue, *Plant J*. 19 (1999) 229–236. doi:10.1046/j.1365-313X.1999.00512.x.
- [6] Z. Lin, K.L. Solomon, X. Zhang, N.J. Pavlos, T. Abel, C. Willers, K. Dai, J. Xu, Q. Zheng, M. Zheng, In vitro evaluation of natural marine sponge collagen as a scaffold for bone tissue engineering, *Int. J. Biol. Sci.* 7 (2011) 968–977. doi:10.7150/ijbs.7.968.
- [7] N. Leventis, C. Sotiriou-Leventis, G. Zhang, A.M.M. Rawashdeh, Nanoengineering Strong Silica Aerogels, *Nano Lett.* 2 (2002) 957–960. doi:10.1021/nl025690e.
- [8] T.M. Tillotson, L.W. Hrubesh, Transparent ultralow-density silica aerogels prepared by a two-step sol-gel process, *J. Non. Cryst. Solids*. 145 (1992) 44–50. doi:10.1016/S0022-3093(05)80427-2.
- [9] M.A. Worsley, S.O. Kucheyev, J.H. Satcher, A. V. Hamza, T.F. Baumann, Mechanically robust and electrically conductive carbon nanotube foams, *Appl. Phys. Lett.* 94 (2009) 1–4. doi:10.1063/1.3086293.
- [10] Z. Qin, G.S. Jung, M.J. Kang, M.J. Buehler, The mechanics and design of a lightweight three-dimensional graphene assembly, *Sci. Adv.* 3 (2017) 1–8. doi:10.1126/sciadv.160153.
- [11] F. Scarpa, L.G. Ciffo, J.R. Yates, Dynamic properties of high structural integrity auxetic open cell foam, *Smart Mater. Struct.* 13 (2004) 49–56. doi:10.1088/0964-1726/13/1/006.
- [12] M. Letellier, C. Delgado-Sanchez, M. Khelifa, V. Fierro, A. Celzard, Mechanical properties of model vitreous carbon foams, *Carbon N. Y.* 116 (2017) 562–571. doi:10.1016/j.carbon.2017.02.020.
- [13] R.W. Pekala, C.T. Alviso, J.D. LeMay, Organic aerogels: microstructural dependence of

- mechanical properties in compression, *J. Non. Cryst. Solids*. 125 (1990) 67–75.
doi:10.1016/0022-3093(90)90324-F.
- [14] X. Zheng, H. Lee, T.H. Weisgraber, M. Shusteff, J. DeOtte, E.B. Duoss, J.D. Kuntz, M.M. Biener, Q. Ge, J. a Jackson, S.O. Kucheyev, N.X. Fang, C.M. Spadaccini, Ultralight, ultrastiff mechanical metamaterials., *Science*. 344 (2014) 1373–1377.
doi:10.1126/science.1252291.
- [15] T. a. Schaedler, a. J. Jacobsen, a. Torrents, a. E. Sorensen, J. Lian, J.R. Greer, L. Valdevit, W.B. Carter, Ultralight Metallic Microlattices, *Science* (80-.). 334 (2011) 962–965. doi:10.1126/science.1211649.
- [16] J. Bauer, A. Schroer, R. Schwaiger, O. Kraft, Approaching theoretical strength in glassy carbon nanolattices, *Nat. Mater.* 15 (2016) 438–443. doi:10.1038/nmat4561.
- [17] A. Szczurek, A. Ortona, L. Ferrari, E. Rezaei, G. Medjahdi, V. Fierro, D. Bychanok, P. Kuzhir, A. Celzard, Carbon periodic cellular architectures, *Carbon N. Y.* 88 (2015) 70–85. doi:10.1016/j.carbon.2015.02.069.
- [18] L. Valdevit, A.J. Jacobsen, J.R. Greer, W.B. Carter, Protocols for the optimal design of multi-functional cellular structures: From hypersonics to micro-architected materials, *J. Am. Ceram. Soc.* 94 (2011) 15–34. doi:10.1111/j.1551-2916.2011.04599.x.
- [19] T.A. Schaedler, C.J. Ro, A.E. Sorensen, Z. Eckel, S.S. Yang, W.B. Carter, A.J. Jacobsen, Designing metallic microlattices for energy absorber applications, *Adv. Eng. Mater.* 16 (2014) 276–283. doi:10.1002/adem.201300206.
- [20] O.-Y. Kwon, H.-J. Ryu, S.-Y. Jeong, Porous layered carbon as catalyst support material for PEMFC, *J. Ind. Eng. Chem.* 12 (2006) 306–310.
- [21] R.A. Olson, L.C.B. Martins, Cellular ceramics in metal filtration, *Adv. Eng. Mater.* 7 (2005) 187–192. doi:10.1002/adem.200500021.
- [22] M. Inagaki, J. Qiu, Q. Guo, Carbon foam: Preparation and application, *Carbon N. Y.* 87 (2015) 128–152. doi:10.1016/j.carbon.2015.02.021.
- [23] C. Chen, E.B. Kennel, A.H. Stiller, P.G. Stansberry, J.W. Zondlo, Carbon foam derived

- from various precursors, *Carbon* N. Y. 44 (2006) 1535–1543.
doi:10.1016/j.carbon.2005.12.021.
- [24] G. Tondi, a Pizzi, R. Olives, Natural Tannin-Based Rigid Foams As Insulation for Doors and Wall Panels, *Maderas. Cienc. Y Tecnol.* 10 (2008) 219–227. doi:10.4067/S0718-221X2008000300005.
- [25] L.H. Dudte, E. Vouga, T. Tachi, L. Mahadevan, Programming curvature using origami tessellations, *Nat. Mater.* 15 (2016) 583–588. doi:10.1038/nmat4540.
- [26] D. Dureisseix, An Overview of Mechanisms and Patterns with Origami, *Int. J. Sp. Struct.* 27 (2012) 1–14. doi:10.1260/0266-3511.27.1.1.
- [27] A. Lebéé, From folds to structures, a review, *Int. J. Sp. Struct.* 30 (2015) 55–74. doi:10.1260/0266-3511.30.2.55.
- [28] M. Schenk, S.D. Guest, Origami folding: A structural engineering approach., in: *Origami 5 Fifth Int. Meet. Origami Sci. Math.*, CRC Press, Boca Raton, FL., 2011: pp. 291–304.
- [29] T. Tachi, Geometric Considerations for the Design of Rigid Origami Structures, *Proceedings Int. Assoc. Shell Spat. Struct. Symp.* 2010. 12 (2010) 458–460. doi:10.1016/j.mpaic.2011.07.005.
- [30] C. Lv, D. Krishnaraju, G. Konjevod, H. Yu, H. Jiang, Origami based Mechanical Metamaterials., *Sci. Rep.* 4 (2014) 5979. doi:10.1038/srep05979.
- [31] K.C. Cheung, T. Tachi, S. Calisch, K. Miura, Origami interleaved tube cellular materials, *Smart Mater. Struct.* 23 (2014) 94012. doi:10.1088/0964-1726/23/9/094012.
- [32] S. Fischer, K. Drechsler, S. Kilchert, A. Johnson, Mechanical tests for foldcore base material properties, *Compos. Part A Appl. Sci. Manuf.* 40 (2009) 1941–1952. doi:10.1016/j.compositesa.2009.03.005.
- [33] H. Yasuda, C. Chong, E.G. Charalampidis, P.G. Kevrekidis, J. Yang, Formation of rarefaction waves in origami-based metamaterials, *Phys. Rev. E - Stat. Nonlinear, Soft Matter Phys.* 93 (2016) 1–11. doi:10.1103/PhysRevE.93.043004.
- [34] S. Heimbs, J. Cichosz, M. Klaus, S. Kilchert, A.F. Johnson, Sandwich structures with

- textile-reinforced composite foldcores under impact loads, *Compos. Struct.* 92 (2010) 1485–1497. doi:10.1016/j.compstruct.2009.11.001.
- [35] Z.Y. Wei, Z. V. Guo, L. Dudte, H.Y. Liang, L. Mahadevan, Geometric mechanics of periodic pleated origami, *Phys. Rev. Lett.* 110 (2013) 1–5. doi:10.1103/PhysRevLett.110.215501.
- [36] M. Schenk, S.D. Guest, Geometry of Miura-folded metamaterials, *Proc. Natl. Acad. Sci.* 110 (2013) 3276–3281. doi:10.1073/pnas.1217998110.
- [37] K. Miura, *Method of packaging and deployment of large membranes in space*, 1985.
- [38] Z. Song, T. Ma, R. Tang, Q. Cheng, X. Wang, D. Krishnaraju, R. Panat, C.K. Chan, H. Yu, H. Jiang, Origami lithium-ion batteries, *Nat. Commun.* 5 (2014) 1–6. doi:10.1038/ncomms4140.
- [39] T. Street, Deployable membranes designed, *Philos. Trans. R. Soc. A.* 360 (2002) 227–238. doi:10.1098/rsta.2001.0928.
- [40] H. Kobayashi, B. Kresling, J.F. V. Vincent, The geometry of unfolding tree leaves, *Proc. R. Soc. B Biol. Sci.* 265 (1998) 147–154. doi:10.1098/rspb.1998.0276.
- [41] M. Ben Amar, F. Jia, Anisotropic growth shapes intestinal tissues during embryogenesis, *Proc. Natl. Acad. Sci.* 110 (2013) 10525–10530. doi:10.1073/pnas.1217391110.
- [42] F. Haas, R.J. Wootton, Two basic mechanisms in insect wing folding, *Proc. R. Soc. London B Biol. Sci.* 263 (1996) 1651–1658.
- [43] E.A. Peraza-Hernandez, D.J. Hartl, R.J. Malak Jr, D.C. Lagoudas, Origami-inspired active structures: a synthesis and review, *Smart Mater. Struct.* 23 (2014) 94001. doi:10.1088/0964-1726/23/9/094001.
- [44] C.E. Byrne, D.C. Nagle, *Carbonization of Wood for Advanced Materials Applications*, *Carbon N. Y.* 35 (1991) 259–266. doi:10.1016/S0008-6223(96)00136-4.
- [45] Y. Liang, D. Wu, R. Fu, Carbon microfibers with hierarchical porous structure from electrospun fiber-like natural biopolymer, *Sci. Rep.* 3 (2013) 1–5. doi:10.1038/srep01119.

- [46] Y. Wang, L. Pham, G.P.S. De Vasconcellos, M. Madou, Fabrication and characterization of micro PEM fuel cells using pyrolyzed carbon current collector plates, *J. Power Sources*. 195 (2010) 4796–4803. doi:10.1016/j.jpowsour.2010.02.050.
- [47] M. Islam, R. Natu, M.F. Larraga-Martinez, R. Martinez-Duarte, Enrichment of diluted cell populations from large sample volumes using 3D carbon-electrode dielectrophoresis, *Biomicrofluidics*. 10 (2016). doi:10.1063/1.4954310.
- [48] S.M. Manocha, K. Patel, L.M. Manocha, Development of carbon foam from phenolic resin via template route, *Indian J. Eng. Mater. Sci.* 17 (2010) 338–342.
- [49] S. Callcut, J.C. Knowles, Correlation between structure and compressive strength in a reticulated glass-reinforced hydroxyapatite foam, *J. Mater. Sci. Mater. Med.* 13 (2002) 485–489. doi:10.1023/A:1014718722710.
- [50] A. Celzard, W. Zhao, A. Pizzi, V. Fierro, Mechanical properties of tannin-based rigid foams undergoing compression, *Mater. Sci. Eng. A*. 527 (2010) 4438–4446. doi:10.1016/j.msea.2010.03.091.
- [51] O.J.A. Schueller, S.T. Brittain, C. Marzolin, G.M. Whitesides, Fabrication and Characterization of Glassy Carbon MEMS, *Chem. Mater.* 9 (1997) 1399–1406. <http://dx.doi.org/10.1021/cm960639v>.
- [52] E.E. Hucke, R.A. Fuys, R.G. Craig, Glassy Carbon : A Potential Dental Implant Material, *J. Biomed. Mater. Res. Part A*. 274 (1973) 263–274.
- [53] MatWeb, Vitreous Carbon (Glassy Carbon), (n.d.). <http://www.matweb.com/search/datasheet.aspx?matguid=2f4d47d4e39d4091baa8625d4ed46cb1&ckck=1>.
- [54] M.F. Ashby, D.R.H. Jones, *Engineering Materials 2*, 4th Editio, Elsevier Butterworth-Heinemann, Waltham, MA, 2013.
- [55] M.F. Ashby, The properties of foams and lattices., *Philos. Trans. A. Math. Phys. Eng. Sci.* 364 (2006) 15–30. doi:10.1098/rsta.2005.1678.
- [56] O.M. Istrate, B. Chen, Relative modulus–relative density relationships in low density

- polymer–clay nanocomposite foams, *Soft Matter*. 7 (2011) 1840.
doi:10.1039/c0sm01052a.
- [57] O.J.A. Schueller, S.T. Brittain, G.M. Whitesides, Fabrication of glassy carbon microstructures by soft lithography, *Sensors Actuators A Phys.* 72 (1999) 125–139.
<http://www.sciencedirect.com/science/article/B6THG-3WWKP15-4/2/f3422932275d5954ebd275baad93744c>.
- [58] V.S. Deshpande, N.A. Fleck, Collapse of truss core sandwich beams in 3-point bending, *Int. J. Solids Struct.* 38 (2001) 6275–6305. doi:10.1016/S0020-7683(01)00103-2.
- [59] J. Su, A.C. Lua, Effects of carbonisation atmosphere on the structural characteristics and transport properties of carbon membranes prepared from Kapton?? polyimide, *J. Memb. Sci.* 305 (2007) 263–270.
- [60] M.A. Hubbe, R.A. Venditti, O.J. Rojas, What happens to cellulosic fibers during papermaking and recycling? A review, *BioResources*. 2 (2007) 739–788.
doi:10.15376/biores.2.4.739-788.
- [61] M. Rasi, *Permeability Properties of Paper Materials*, University of Jyväskylä, 2013.
- [62] J.H. Gyres, R. Amiri, D. McDonald, The Specific Pore Volume of Multiplanar Webs: The Role of the Short and Long Fibre Fractions, in: *Sci. Papermak. Trans. XIIth Fund. Res. Symp.*, CF Baker, Oxford, UK, 2001: pp. 1371–1383.
- [63] X.Y. Liu, M. Huang, H.L. Ma, Z.Q. Zhang, J.M. Gao, Y.L. Zhu, X.J. Han, X.Y. Guo, Preparation of a carbon-based solid acid catalyst by sulfonating activated carbon in a chemical reduction process, *Molecules*. 15 (2010) 7188–7196.
doi:10.3390/molecules15107188.
- [64] V. Palmre, E. Lust, A. Jänes, M. Koel, A.-L. Peikolainen, J. Torop, U. Johanson, A. Aabloo, Electroactive polymer actuators with carbon aerogel electrodes, *J. Mater. Chem.* 21 (2011) 2577. doi:10.1039/c0jm01729a.
- [65] J.G. Giuliani, T.E. Benavidez, G.M. Duran, E. Vinogradova, A. Rios, C.D. Garcia, Development and characterization of carbon based electrodes from pyrolyzed paper for

- biosensing applications, *J. Electroanal. Chem.* 765 (2016) 8–15.
doi:10.1016/j.jelechem.2015.07.055.
- [66] I. Keun Kwon, S. Kidoaki, T. Matsuda, Electrospun nano- to microfiber fabrics made of biodegradable copolyesters: Structural characteristics, mechanical properties and cell adhesion potential, *Biomaterials*. 26 (2005) 3929–3939.
doi:10.1016/j.biomaterials.2004.10.007.
- [67] C.L. Pai, M.C. Boyce, G.C. Rutledge, Mechanical properties of individual electrospun PA 6(3)T fibers and their variation with fiber diameter, *Polymer (Guildf)*. 52 (2011) 2295–2301. doi:10.1016/j.polymer.2011.03.041.
- [68] S.S. Munawar, K. Umemura, S. Kawai, Characterization of the morphological, physical, and mechanical properties of seven nonwood plant fiber bundles, *J. Wood Sci.* 53 (2007) 108–113. doi:10.1007/s10086-006-0836-x.
- [69] W.M.A.W. Daud, W.S.W. Ali, M.Z. Sulaiman, Effects of carbonization temperature on pore development in palm-shell-based activated carbon, *Carbon N. Y.* 38 (2000) 1925–1932. doi:10.1016/S0008-6223(00)00028-2.
- [70] J. de D. Lopez-Gonzalez, F. Martinez-Vilchez, F. Rodriguez-Reinoso, J.D.D. Lopez-Gonzalez, Preparation and characterization of active carbons from olive stones., *Sect. Title Inorg. Chem. React.* 18 (1980) 413–418. doi:10.1016/0008-6223(80)90033-0.
- [71] Y. Li, C.T. Lim, M. Kotaki, Study on structural and mechanical properties of porous PLA nanofibers electrospun by channel-based electrospinning system, *Polym. (United Kingdom)*. 56 (2015) 572–580. doi:10.1016/j.polymer.2014.10.073.
- [72] W. Li, K. Yang, J. Peng, L. Zhang, S. Guo, H. Xia, Effects of carbonization temperatures on characteristics of porosity in coconut shell chars and activated carbons derived from carbonized coconut shell chars, *Ind. Crops Prod.* 28 (2008) 190–198.
doi:10.1016/j.indcrop.2008.02.012.
- [73] Y. Liu, J. Zhou, E. Zhu, J. Tang, X. Liu, W. Tang, Facile synthesis of bacterial cellulose fibres covalently intercalated with graphene oxide by one-step cross-linking for robust supercapacitors, *J. Mater. Chem. C*. 3 (2015) 1011–1017. doi:10.1039/C4TC01822B.

- [74] M. Poletto, V. Pistor, M. Zeni, A.J. Zattera, Crystalline properties and decomposition kinetics of cellulose fibers in wood pulp obtained by two pulping processes, *Polym. Degrad. Stab.* 96 (2011) 679–685. doi:10.1016/j.polymdegradstab.2010.12.007.
- [75] M.S. Mettler, S.H. Mushrif, A.D. Paulsen, A.D. Javadekar, D.G. Vlachos, P.J. Dauenhauer, Revealing pyrolysis chemistry for biofuels production: Conversion of cellulose to furans and small oxygenates, *Energy Environ. Sci.* 5 (2012) 5414. doi:10.1039/c1ee02743c.
- [76] D.K. Shen, S. Gu, The mechanism for thermal decomposition of cellulose and its main products, *Bioresour. Technol.* 100 (2009) 6496–6504. doi:10.1016/j.biortech.2009.06.095.
- [77] D. Shen, R. Xiao, S. Gu, H. Zhang, The Overview of Thermal Decomposition of Cellulose in Lignocellulosic Biomass, in: *Cellul. - Biomass Convers.*, 2013: pp. 193–226. doi:10.5772/51883.
- [78] S. Li, J. Lyons-Hart, J. Banyasz, K. Shafer, Real-time evolved gas analysis by FTIR method: An experimental study of cellulose pyrolysis, *Fuel.* 80 (2001) 1809–1817. doi:10.1016/S0016-2361(01)00064-3.
- [79] M. Iwaki, K. Terashima, Change in atomic density of glassy carbon by Na ion implantation, *Surf. Coatings Technol.* 128–129 (2000) 429–433.
- [80] H. Chen, *Biotechnology of lignocellulose: Theory and practice*, 2014. doi:10.1007/978-94-007-6898-7.
- [81] A. Bejan, Forced convection: Internal flows, in: A. Bejan, A. Kraus (Eds.), *Heat Transf. Handb.*, John Wiley & Sons, Inc., 2003: pp. 395–438.
- [82] B. Dickens, Thermally degrading polyethylene studied by means of factor-jump thermogravimetry, *J. Polym. Sci. Polym. Chem. Ed.* 20 (1982) 1065–1087.
- [83] W.S. Kwon, K.W. Paik, Fundamental understanding of ACF conduction establishment with emphasis on the thermal and mechanical analysis, *Int. J. Adhes. Adhes.* 24 (2004) 135–142. doi:10.1016/j.ijadhadh.2003.07.003.
- [84] A. Gardziella, L.A. Pilato, A. Knop, *Phenolic resins- Chemistry, applications*,

standardization, safety and ecology, Springer Berlin Heidelberg, 2000.

- [85] X. Wang, Q. Zhu, S.M. Mahurin, C. Liang, S. Dai, Preparation of free-standing high quality mesoporous carbon membranes, *Carbon N. Y.* 48 (2010) 557–560. doi:10.1016/j.carbon.2009.09.059.
- [86] J. Laine, A. Calafat, M. Labady, Preparation and Characterization of Activated Carbons From Coconut Shell Impregnated With Phosphoric-Acid, *Carbon N. Y.* 27 (1989) 191–195. doi:10.1016/0008-6223(89)90123-1.
- [87] D.H. Page, R.S. Seth, B.D. Jordan, M.C. Barbe, Curl, crimps, kinks and microcompressions in pulp fibres: Their origin, measurement and significance, in: *Papermak. Raw Mater. Trans. 8th Fundam. Res. Symp.*, 1985: pp. 183–227. <http://www.ppfrs.org/PageSethJordanBarbe1985.pdf>.
- [88] A. Namiki, S. Yokosawa, Robotic origami folding with dynamic motion primitives, *IEEE Int. Conf. Intell. Robot. Syst.* 2015–Decem (2015) 5623–5628. doi:10.1109/IROS.2015.7354175.
- [89] K. Tanaka, Y. Kamotani, Y. Yokokohji, Origami folding by a robotic hand, *IEEE Int. Conf. Intell. Robot. Syst.* (2007) 2540–2547. doi:10.1109/IROS.2007.4399358.
- [90] H. Liu, J. Dai, An approach to carton-folding trajectory planning using dual robotic fingers, *Rob. Auton. Syst.* 42 (2003) 47–63. doi:10.1016/S0921-8890(02)00312-3.
- [91] C. Zhao, Q. Peng, P. Gu, Development of a paper-bag-folding machine using open architecture for adaptability, *Proc. Inst. Mech. Eng. Part B J. Eng. Manuf.* 229 (2015) 954405414559281. doi:10.1177/0954405414559281.
- [92] K.L. Corcoran, CREASE AND EMBOSsing DIE, US 2005/0215405 A1, 2005.
- [93] P.W. Jarrett, D.M. Jarrett, ROLLERS FOR CUTTING, CREAMING, PERFORATING OR EMBOSsing SHEET MATERIALS, 3,744,384, 1973.
- [94] E. Cavagna, DEVICE FOR EMBOSsing AND/OR CREAMING SHEET, OR ROLL MATERIAL, 4,641,575, 1987.
- [95] H. Celik, S. Samanli, Ö. Öney, The use of tincal calcination plant waste as an additive in

- ceramic wall tile production, *J. Ceram. Process. Res.* 15 (2014) 508–513.
- [96] H. Zhuo, Y. Hu, X. Tong, L. Zhong, X. Peng, R. Sun, Sustainable Hierarchical Porous Carbon Aerogel from Cellulose for High-Performance Supercapacitor and CO₂ Capture, *Ind. Crops Prod.* 87 (2016) 229–235. doi:10.1016/j.indcrop.2016.04.041.
- [97] S. Li, G. Ren, M.N.F. Hoque, Z. Dong, J. Warzywoda, Z. Fan, Carbonized cellulose paper as an effective interlayer in lithium-sulfur batteries, *Appl. Surf. Sci.* 396 (2017) 637–643. doi:10.1016/j.apsusc.2016.10.208.
- [98] G.M. Duran, T.E. Benavidez, J.G. Giuliani, A. Rios, C.D. Garcia, Synthesis of CuNP-modified carbon electrodes obtained by pyrolysis of paper, *Sensors Actuators, B Chem.* 227 (2016) 626–633. doi:10.1016/j.snb.2015.12.093.
- [99] J. Cai, H. Niu, Z. Li, Y. Du, P. Cizek, Z. Xie, H. Xiong, T. Lin, High-Performance Supercapacitor Electrode Materials from Cellulose-Derived Carbon Nanofibers, *ACS Appl. Mater. Interfaces.* 7 (2015) 14946–14953. doi:10.1021/acsami.5b03757.
- [100] R. Narasimman, K. Prabhakaran, Preparation of carbon foams with enhanced oxidation resistance by foaming molten sucrose using a boric acid blowing agent, *Carbon N. Y.* 55 (2013) 305–312. doi:10.1016/j.carbon.2012.12.068.
- [101] T. V Johnson, Diesel Emission Control in Review, *SAE Int.* 2007-01-0233. 2007 (2007). doi:2007-01-0233.
- [102] W.J. Smothers, J.W. Brockmeyer, L.S. Aubrey, Application of Ceramic Foam Filters in Molten Metal Filtration, in: *Appl. Refract. Ceram. Eng. Sci. Proc.*, 1987: pp. 63–74.